Electronic Supplementary Information

Ultrafast electron and hole transfer dynamics of a solar cell dye containing hole acceptors on mesoporous TiO_2 and Al_2O_3

Mirko Scholz,[a] Oliver Flender,[a] Gerrit Boschloo,[b] Kawon Oum[a] and Thomas Lenzer*[a]*

[a] Universität Siegen, Physikalische Chemie, Adolf-Reichwein-Str. 2, 57076 Siegen, Germany, E-mail: oum@chemie.uni-siegen.de, lenzer@chemie.uni-siegen.de

[b] Department of Chemistry-Ångström Laboratory, Center of Molecular Devices, Uppsala University, Box 523 751 20, Uppsala, Sweden, E-mail: gerrit.boschloo@kemi.uu.se

Table of Contents

Steady-state absorption and fluorescence spectra

Figure S1 shows steady-state absorption spectra of E6 in diisopropyl ether in the region of the $S_0 \rightarrow S_1$/ICT absorption band and the corresponding steady-state fluorescence spectra. Small amounts of acetic acid were systematically added to study the acid/base equilibrium of E6 in this solvent. The shape of the absorption spectra does not change, indicating that the acid is the dominant form in each case. The shape of the fluorescence spectra is also very similar. We only observe a tiny decrease in amplitude with increasing amount of acetic acid. This indicates that the concentration of the anion is further diminished and that the anion has a larger fluorescence quantum yield. This is in agreement with the fluorescence spectra of E6 in acetone reported below. The Stokes shift of E6 in diisopropyl ether is 5200 cm^{-1}.

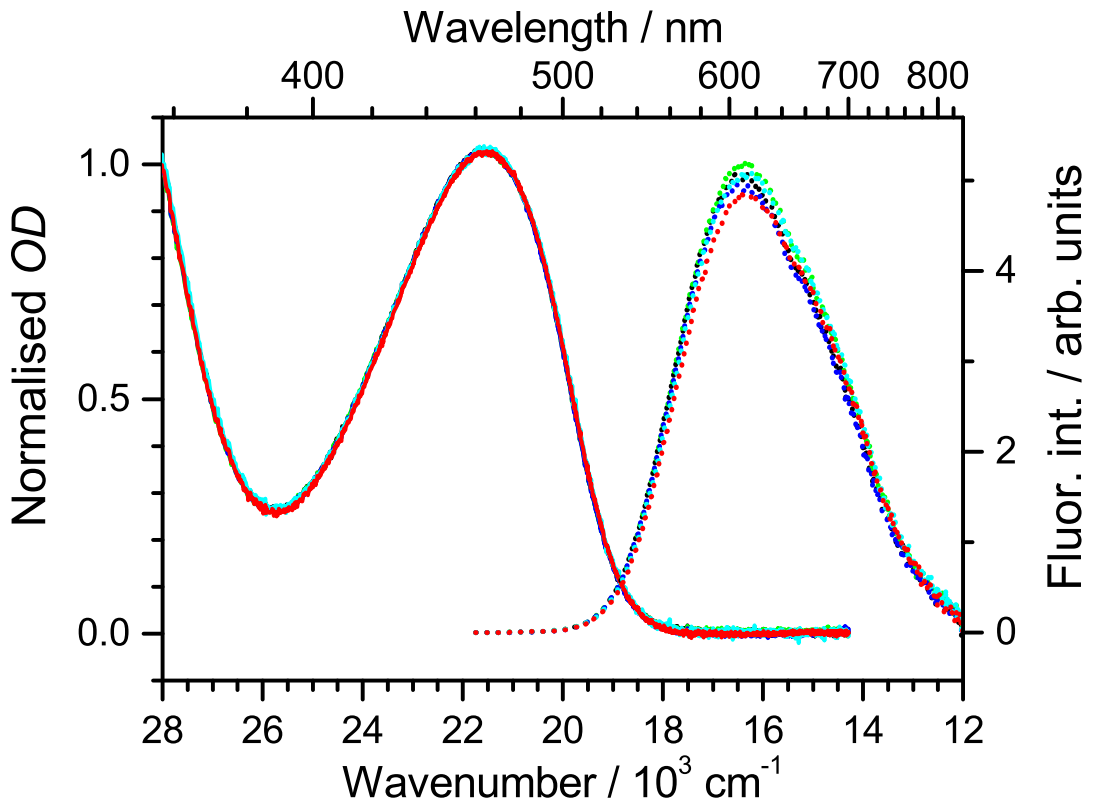

Fig. S1 Comparison of steady-state absorption and fluorescence spectra of E6 in diisopropyl ether. Amount of acetic acid added to 3.00 mL of a 1.5 μM E6 solution: (black) 0, (green) 0.5 μL, (blue) 1 μL, (cyan) 3 μL and (red) 6 μL. The absorption spectra are normalised at 454 nm (excitation wavelength), and the fluorescence spectra show the corresponding relative change in intensity.

Steady-state absorption spectra of a 1.5 μM solution of E6 in acetone are shown in Fig. S2. At this low concentration, the step-wise addition of acetic acid shifts the absorption spectrum to larger wavelengths, with the formation of an isosbestic point at 440 nm. Obviously, E6 predominantly exists in the anion form, and the acid-base equilibrium shifts toward the protonated form upon addition of the weak acid. A small amount of acetic acid should therefore be added to obtain reliable fluorescence spectra of the acid form at the low concentrations required for fluorescence experiments.

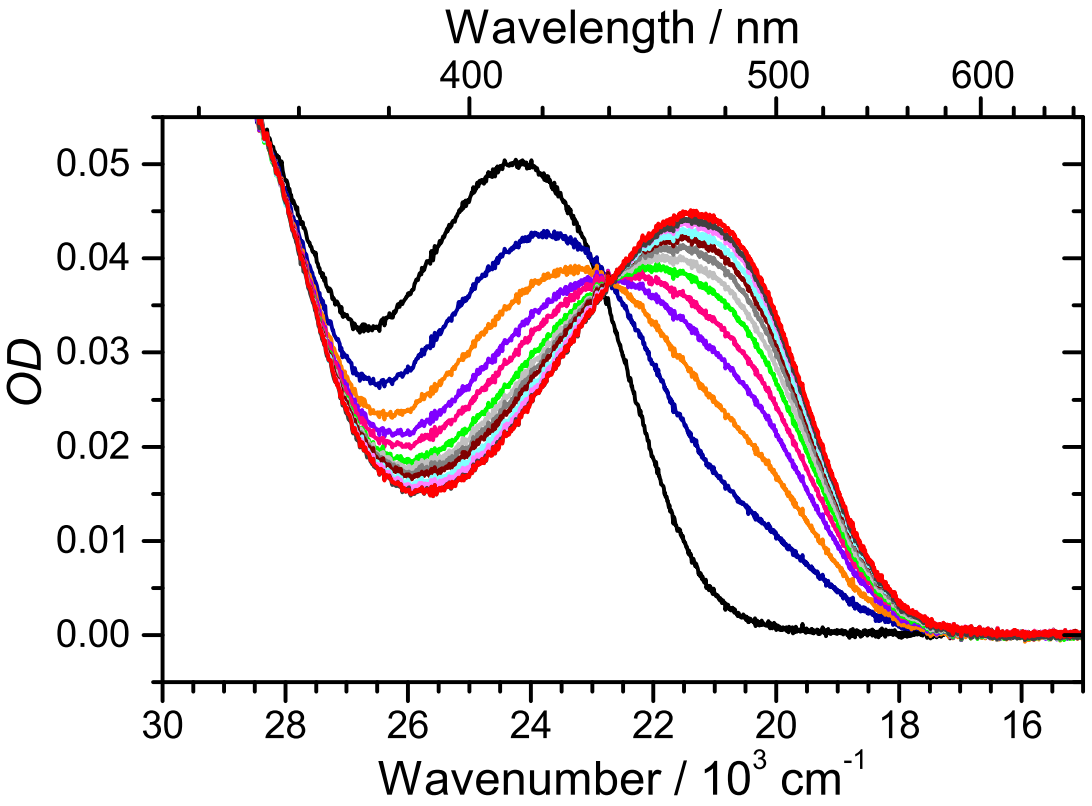

Fig. S2 Steady-state absorption spectra of E6 in acetone with different amounts of acetic acid. Spectra from left to right correspond to the addition of 0 to 6 μL of acetic acid in 0.5 μL steps to 3.00 mL of a 1.5 μM E6 solution. The spectra have been corrected for the dilution effect assuming ideal mixing behaviour.

Steady-state absorption (solid lines) and fluorescence spectra (dotted lines) of E6 in acetone with 0 (black) and 6 μL (red) of acetic acid added are presented in Fig. S3. The shift of the fluorescence spectra follows that of the corresponding absorption spectra. We obtain a Stokes shift of 7250 cm^{-1} for the anion, whereas it is slightly larger in the case of the acid (7900 cm^{-1}). The amplitude of the fluorescence spectra of the acid is smaller. Assuming similar radiative rate constants for the acid and the anion, the excited-state lifetime of the acid should therefore be shorter.

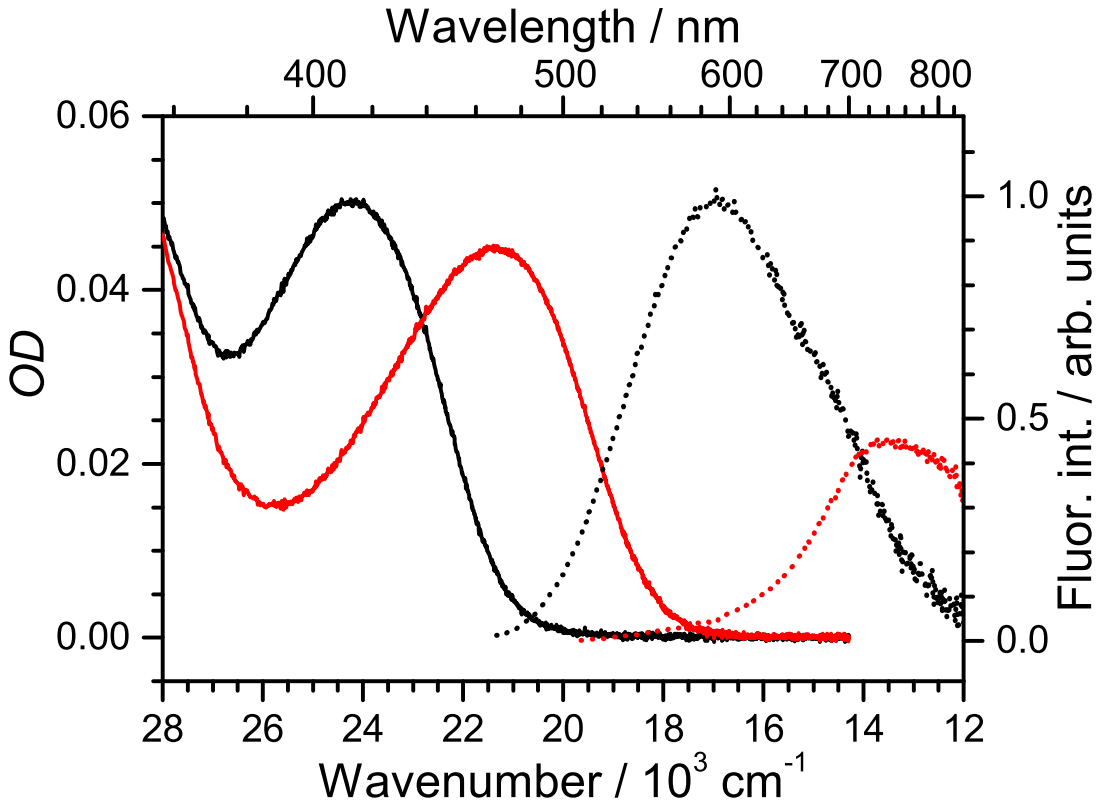

Fig. S3 Steady-state absorption (solid lines) and fluorescence spectra (dotted lines) of E6 in acetone without acetic acid (black) and after addition of 6 μL of acetic acid (red). Fluorescence was excited at 454 and 505 nm, respectively, corresponding to the same *OD* at each excitation wavelength.

Steady-state absorption spectra of E6 in methyl acetate are provided in Fig. S4. Step-wise addition of acetic acid shifts the $S_0 \rightarrow S_1$/ICT band to the red, until the spectrum of the pure acid form is obtained (red line, peak at 470 nm). We recently showed that the band maximum in the UV region (298 nm) is assigned to localised excitation of the pTAA units.[1] Note that the position and shape of this band is largely unaffected by the addition of acid suggesting that the pTAA chromophores are indeed electronically decoupled from the D49 core unit. The change in band intensity is likely due to a higher-energy optical transition of the D49 chromophore contributing to this spectral region.

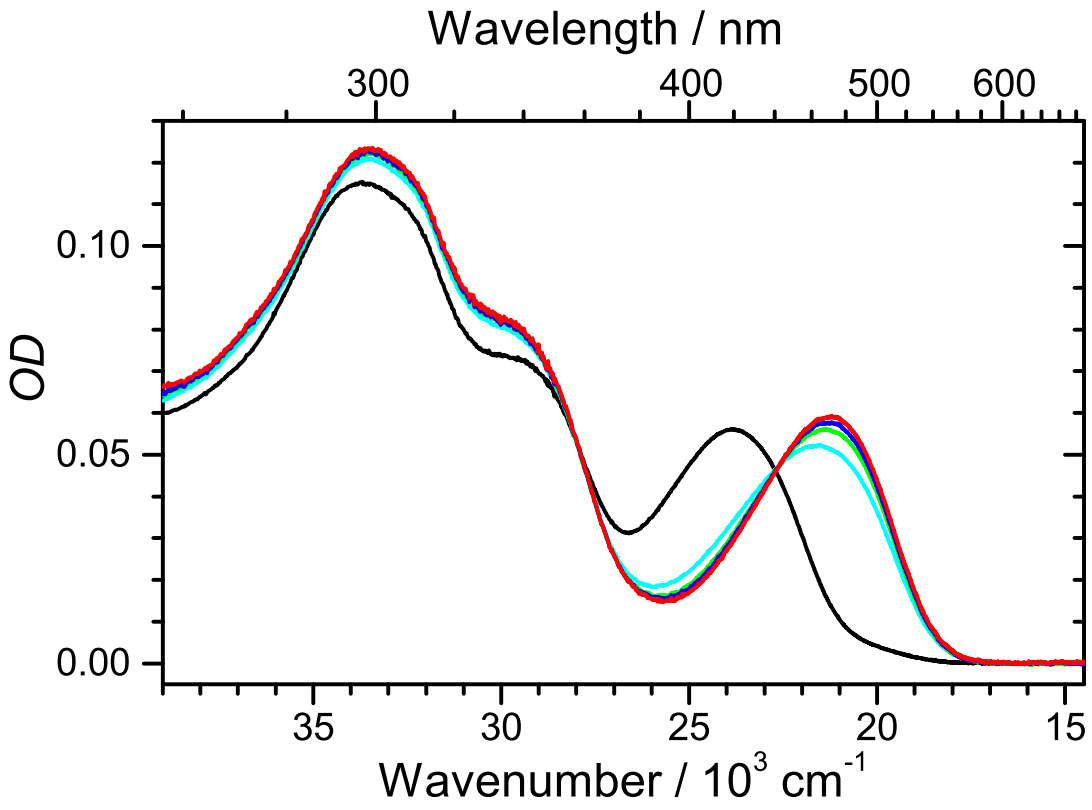

Fig. S4 Steady-state absorption spectra of E6 in methyl acetate with different amounts of acetic acid. Spectra correspond to the addition of 0 (black), 1 (cyan), 2 (green), 3 (blue) and 6 μL (red) of acetic acid to 3.00 mL of a 1.5 μM E6 solution. The spectra have been corrected for the dilution effect assuming ideal mixing behaviour.

Steady-state absorption (solid lines) and fluorescence spectra (dotted lines) of E6 in methyl acetate with 0 (black) and 6 μL (red) of acetic acid added are shown in Fig. S5. The Stokes shift for the anion and the acid is 6250 cm^{-1} and 7150 cm^{-1}, respectively. The amplitude of the fluorescence spectra of the acid is smaller, similar to the behaviour encountered in acetone (Fig. S3). Assuming again similar radiative rate constants for both species, the excited-state lifetime of the acid should be shorter.

Our findings suggest that absorption and fluorescence spectra of E6 and also other solar cell dyes with a conjugated carboxyl anchoring group should be checked routinely for deprotonation. The effect is negligible at higher concentrations in the range of 10^{-4} M typically used in transient absorption experiments. In that case, the acid form prevails. Deprotonation only affects steady-state absorption bands with localised excitation on the D49 core chromophore carrying the carboxyl group, whereas the pTAA groups, to a very good approximation, act as independently absorbing entities.

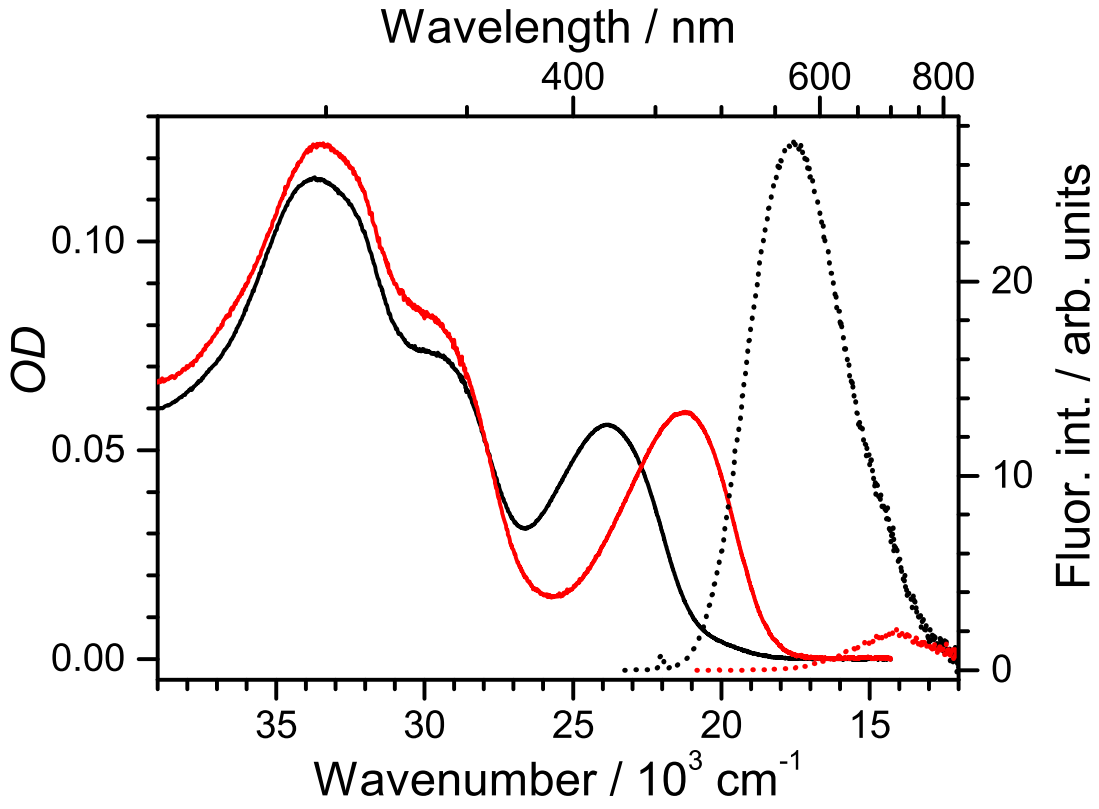

Fig. S5 Steady-state absorption (solid lines) and fluorescence spectra (dotted lines) of E6 in methyl acetate without acetic acid (black) and after addition of 6 μL of acetic acid (red). Fluorescence was excited at 454 and 500 nm, respectively, corresponding to the same *OD* at each excitation wavelength.

Furthermore, spectroelectrochemistry experiments were carried out to obtain steady-state absorption spectra of the cation species. Figure S6 shows cyclic voltammograms for E6/TiO_2/FTO, D49/TiO_2/FTO,[2] and the reference compound ferrocene.[2] As pointed out previously,[2,3] oxidation of D49 occurs at a voltage of 0.51 V *vs.* ferrocene$^+$/ferrocene, *i.e.* 1.14 V *vs.* NHE.[4] In contrast, E6 is oxidised at a slightly lower potential, 0.35 V *vs.* ferrocene$^+$/ferrocene, *i.e.* 0.98 V *vs.* NHE.

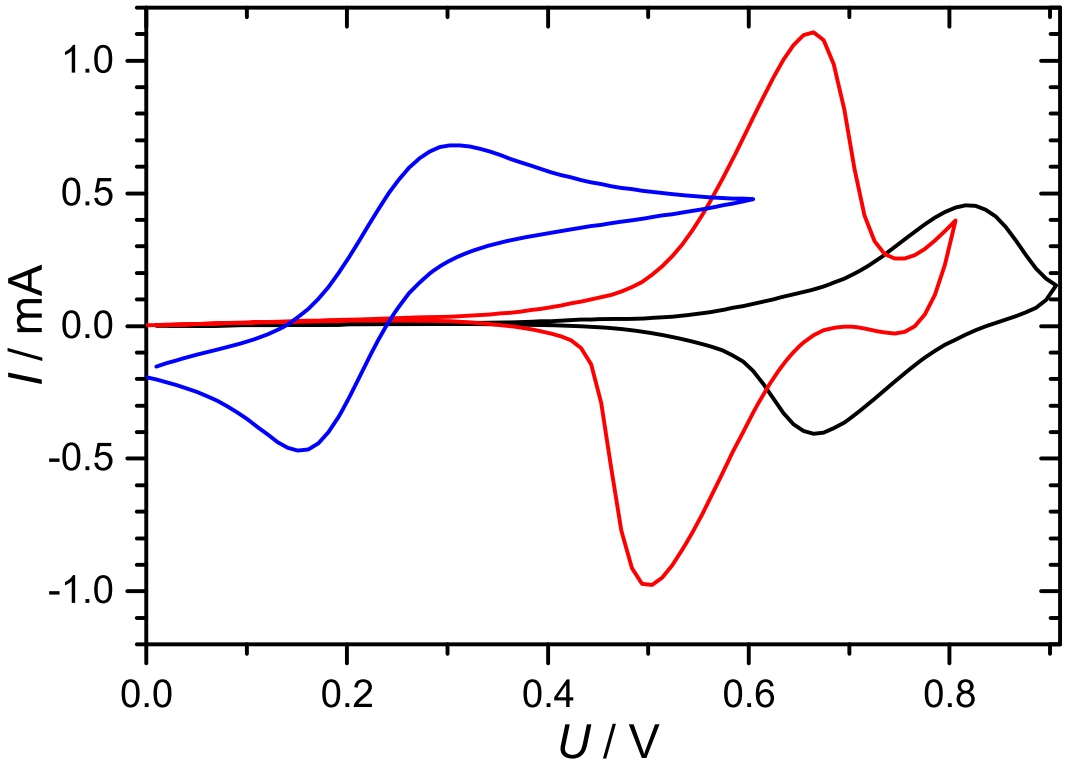

Fig. S6 Cyclic voltammograms for E6/TiO_2/FTO (red), D49/TiO_2/FTO (black),[2] and ferrocene (blue)[2] at a scan rate of 0.1 V s^{-1}.

Figure S7 contains steady-state absorption spectra in the 500-1700 nm region obtained upon oxidation of E6 and D49.[2] For D49/TiO_2/FTO (black line), the peak at 1145 nm was previously assigned to the $D_0 \rightarrow D_1$ transition of the radical cation $D49^{\bullet+}$.[2] For E6/TiO_2/FTO, the first step involves oxidation of both pTAA groups of E6 resulting in formation of a biradical dication $pTAA^{\bullet+}$–D49–$pTAA^{\bullet+}$. The $pTAA^{\bullet+}$ absorption peaks at 722 nm (red line) which is close to the peak position in acetonitrile (730 nm).[1] The spectral FWHM of $pTAA^{\bullet+}$ for the surface-bound E6 species is larger (2460 cm^{-1}) than observed previously in acetonitrile (1670 cm^{-1}).[1] Further oxidation at a higher voltage of 1.30 V, leads to the disappearance of the $pTAA^{\bullet+}$ peak and the formation of two new peaks (blue line): One is located at 1036 nm (FWHM 3690 cm^{-1}) and assigned to the core-oxidised unit ($D49^{\bullet+}$). The corresponding peak of this $D_0 \rightarrow D_1$ transition in acetonitrile was previously found at 1090 nm (FWHM 2510 cm^{-1}).[1] The second peak is observed at 555 nm and is assigned to the $S_0 \rightarrow S_1$ transition of the $pTAA^{2+}$ dication, in very good agreement with previous experiments of Lambert and co-workers for triarylamines in solution.[5] There is no residual $pTAA^{\bullet+}$ signal, thus the oxidised species must be the E6 radical pentacation ($pTAA^{2+}$–$D49^{\bullet+}$– $pTAA^{2+}$).

We note that the second oxidation step differs from that in acetonitrile solution. In the latter case, only oxidation of the core unit was observed at this voltage, but no simultaneous oxidation of $pTAA^{\bullet+}$.[1] In that case, the E6 triradical trication ($pTAA^{\bullet+}$–$D49^{\bullet+}$–$pTAA^{\bullet+}$) was obtained. In any case, the potentials for core and $pTAA^{\bullet+}$ oxidation are expected to be quite close,[3,5] and therefore the different behaviour upon oxidation is understandable, considering the different environment of E6 in the two experiments.

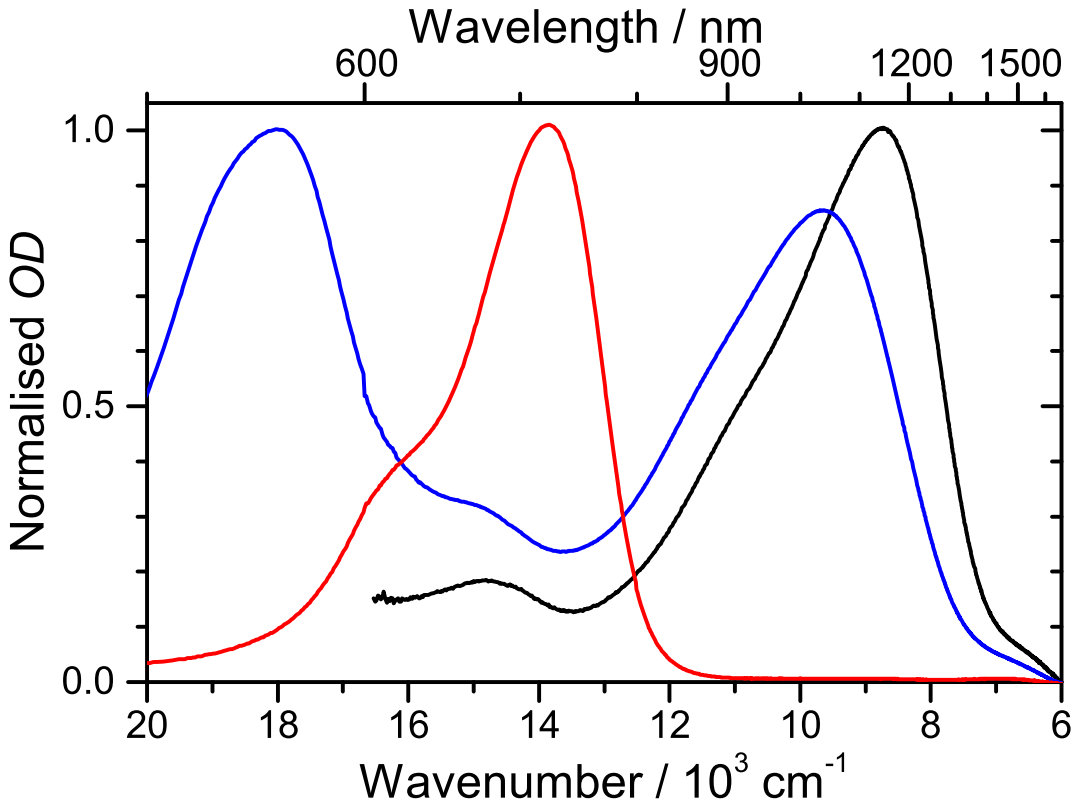

Fig. S7 Comparison of normalised cation spectra from spectroelectrochemistry. (red) $pTAA^{\bullet+}$-D49-$pTAA^{\bullet+}$ biradical dication of E6 on TiO_2/FTO, (blue) E6 radical pentacation ($pTAA^{2+}$-$D49^{\bullet+}$-$pTAA^{2+}$) on TiO_2/FTO, (black) $D49^{\bullet+}$ radical cation on TiO_2/FTO from ref. 1.

Transient absorption spectra

We summarise in Figs. S8-S10 transient absorption spectra of E6 on mesoporous TiO_2 and Al_2O_3 as well as in methyl acetate to better visualise spectral details, complementing the contour plots provided in Fig. 2 (main manuscript). In all cases, E6 was excited by a laser pulse at 500 or 505 nm. Figure S11 shows the PSCP spectra in methyl acetate for the whole UV-Vis-NIR range 260-1600 nm. Note in particular the "selective bleach" of the D49 unit (magenta and blue dotted lines in the bottom panel), whereas the pTAA groups are not involved: The photoexcitation is therefore confined to the D49 core of E6, and the two pTAA substituents are merely spectators.

i) E6/TiO_2/glass

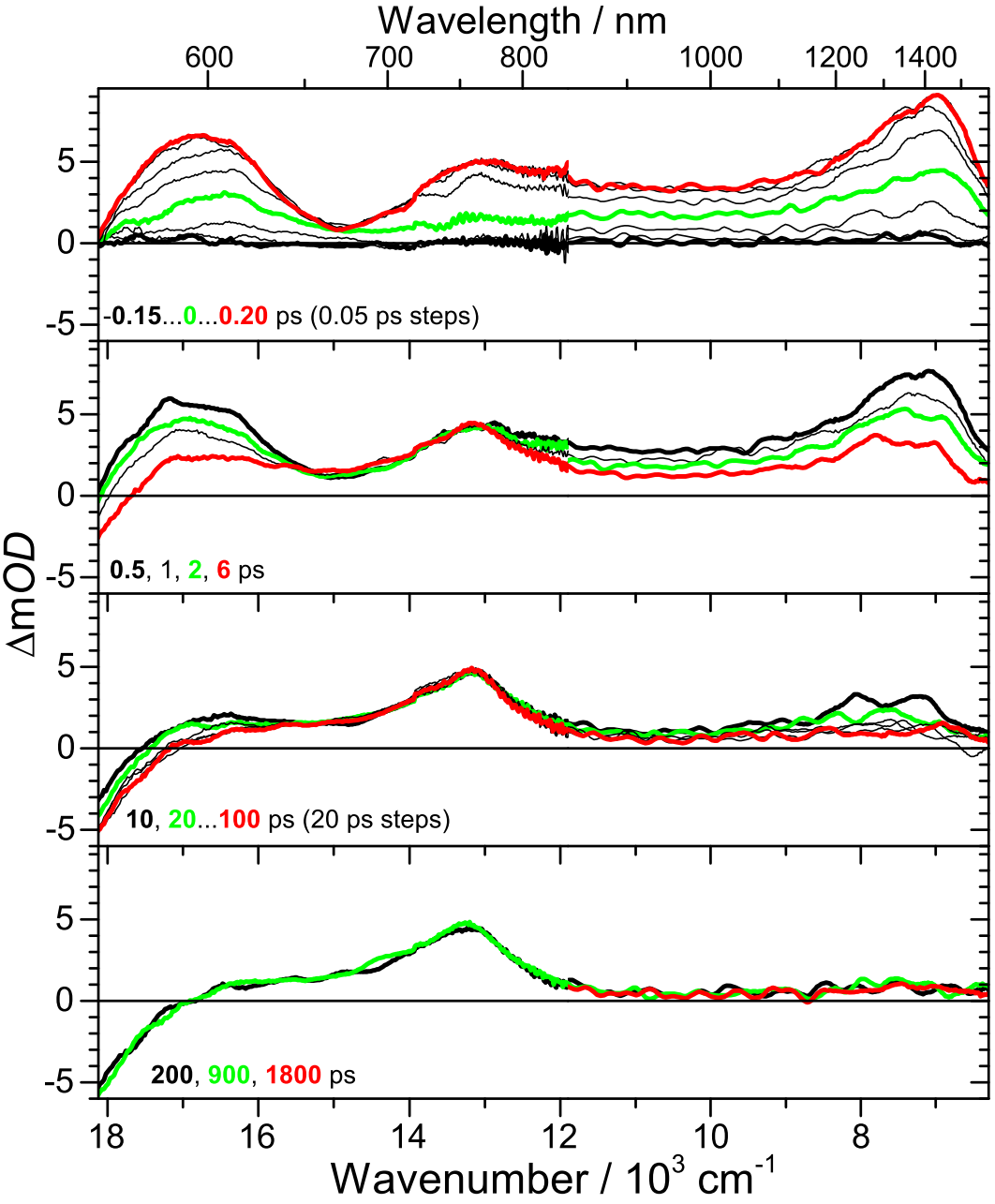

Fig. S8 PSCP transient absorption spectra for E6/TiO_2/glass. (1st panel) -0.15…0…0.20 ps (0.05 ps steps). (2nd panel) 0.5, 1, 2 and 6 ps. (3rd panel) 10 ps and 20…100 ps (20 ps steps). (4th panel) 200, 900 and 1800 ps.

ii) E6/Al_2O_3/glass

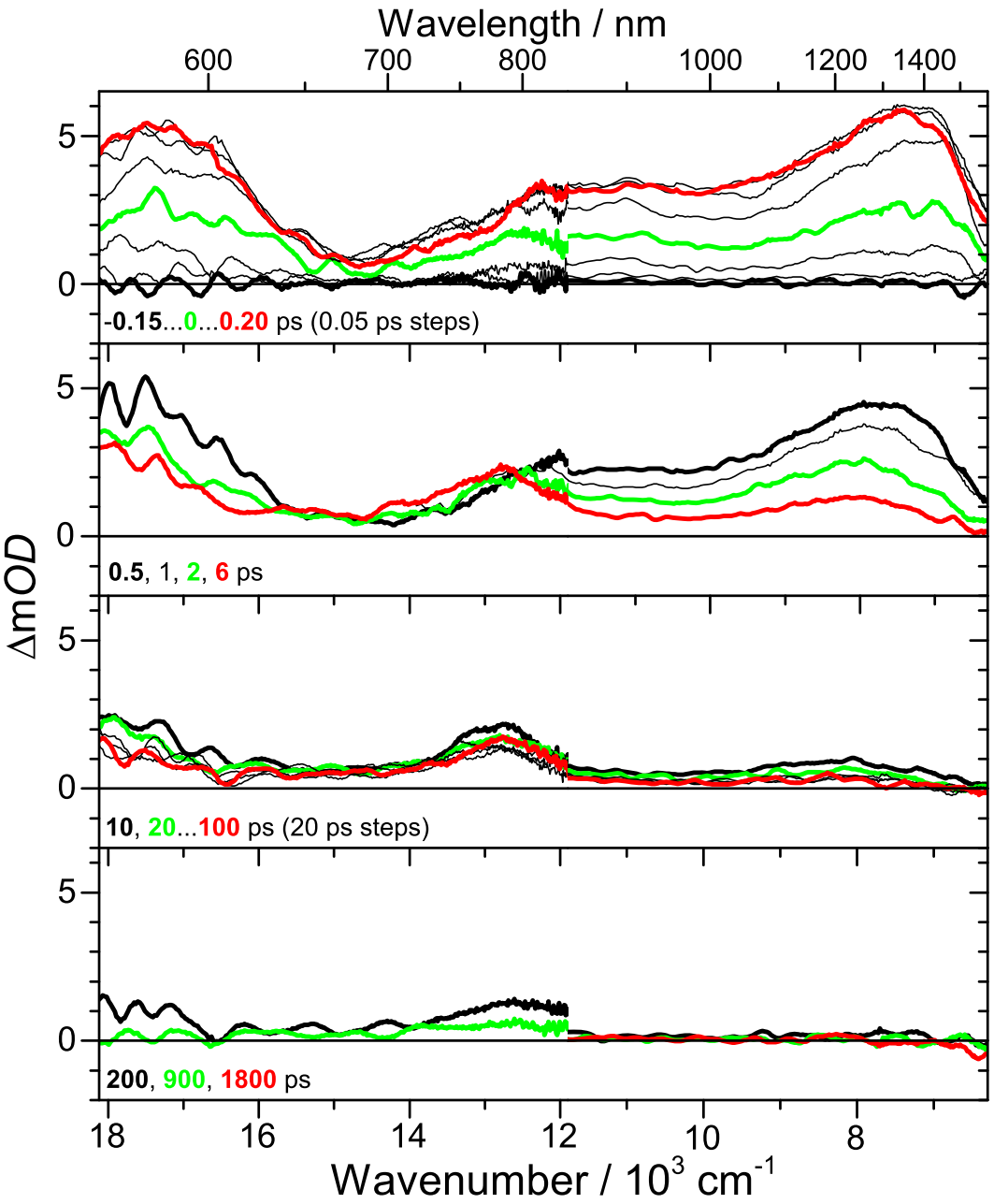

Fig. S9 PSCP transient absorption spectra for E6/Al_2O_3/glass. (1st panel) -0.15…0…0.20 ps (0.05 ps steps). (2nd panel) 0.5, 1, 2 and 6 ps. (3rd panel) 10 ps and 20…100 ps (20 ps steps). (4th panel) 200, 900 and 1800 ps.

iii) E6 in methyl acetate

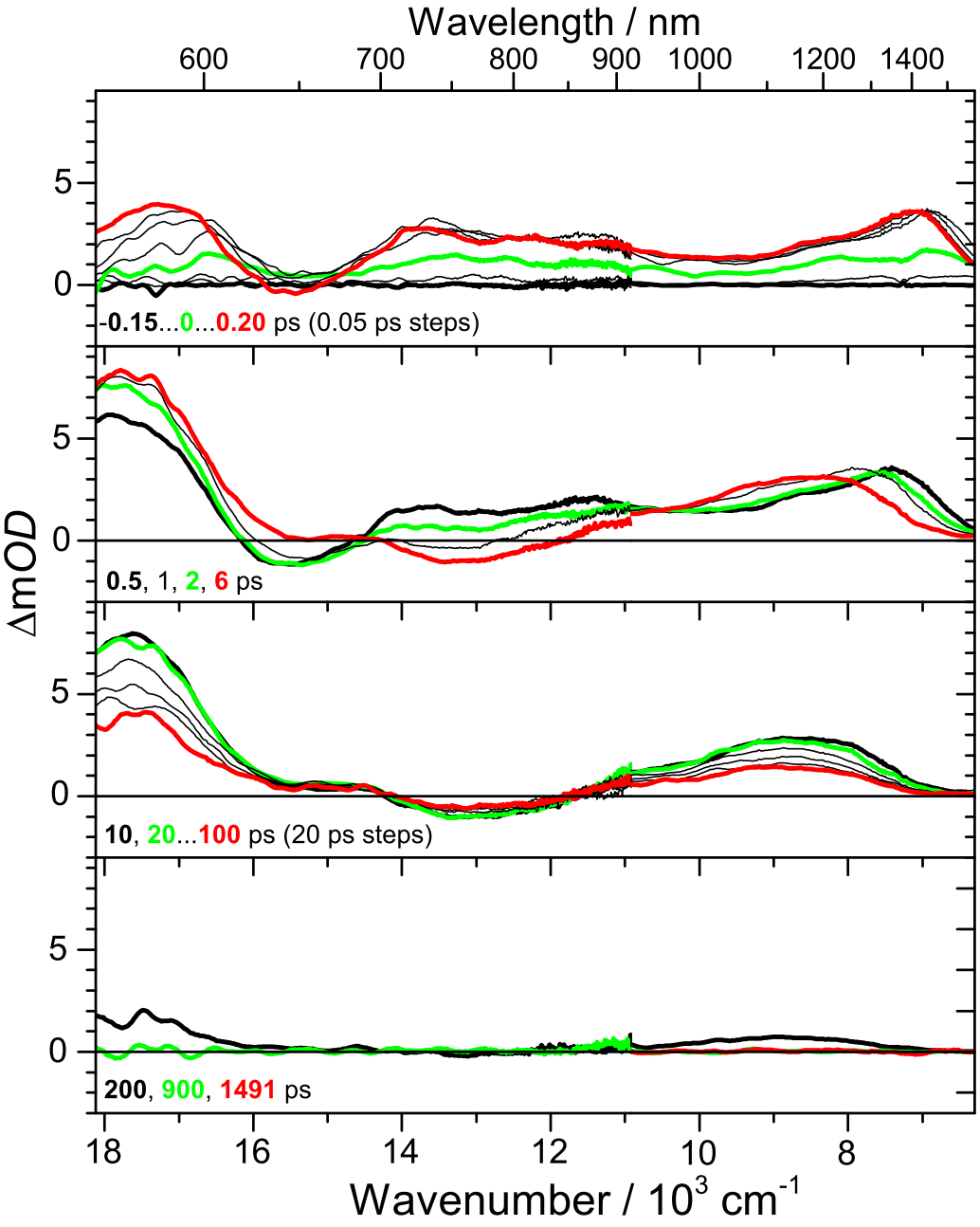

Fig. S10 PSCP transient absorption spectra for E6 in methyl acetate. (1st panel) -0.15…0…0.20 ps (0.05 ps steps). (2nd panel) 0.5, 1, 2 and 6 ps. (3rd panel) 10 ps and 20…100 ps (20 ps steps). (4th panel) 200, 900 and 1491 ps.

iv) E6 in methyl acetate (complete UV-Vis-NIR Range)

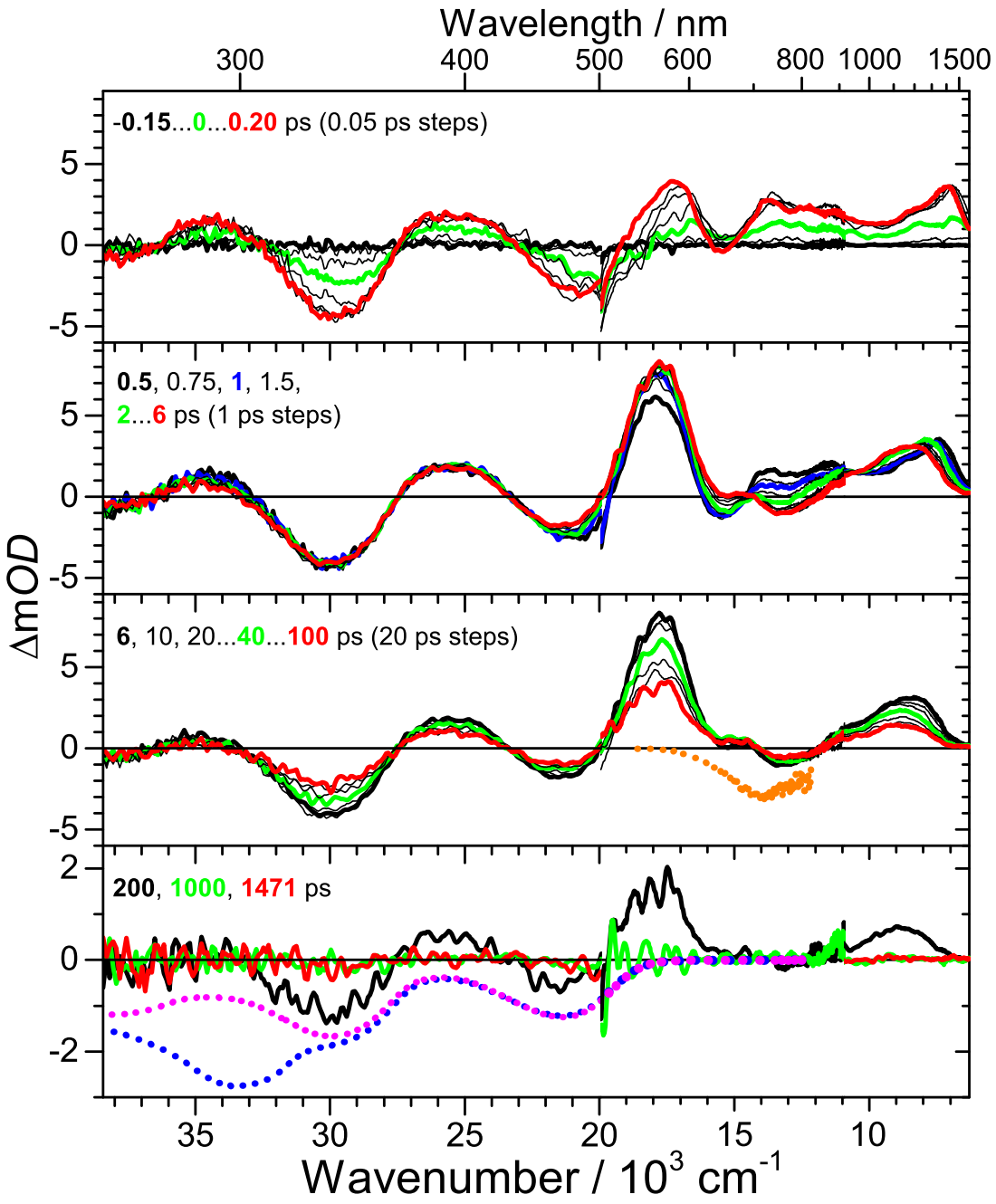

Fig. S11 PSCP transient absorption spectra for E6 in methyl acetate between 260 and 1600 nm. (1st panel) -0.15…0…0.20 ps (0.05 ps steps). (2nd panel) 0.5, 0.75, 1, 1.5 ps and 2…6 ps (1 ps steps). (3rd panel) 6, 10 ps and 20…100 ps (20 ps steps). (4th panel) 200, 1000 and 1471 ps. The blue and magenta dotted lines in the bottom panel are the inverted steady-state absorption spectra of E6 and D49, respectively. Note that only the "D49 part" is bleached. The orange dotted line in the third panel is the steady-state stimulated emission spectrum of E6.

Kinetic traces

Kinetic traces of E6 on TiO_2, Al_2O_3 and in methyl acetate at selected probe wavelengths are compared in Fig. S12 using a logarithmic time scale. A corresponding plot with a linear time scale was already presented in Fig. 3 (main manuscript).

At 560 nm (A), the fast decay for TiO_2 (black) at early times is dominated by the transient Stark effect, and the further decay with smaller amplitude is due to slow hole transfer from $D49^{\bullet+}$ to one of the two pTAA units. The bleach is long-lived, because recombination of $pTAA^{\bullet+}$–D49–pTAA with conduction band electron occurs on much longer timescales. For Al_2O_3 (red), the fast initial decay is due to formation of the radical cation – radical anion species $pTAA^{\bullet+}$–$D49^{\bullet-}$–pTAA, where the remaining absorption contribution is due to the $D49^{\bullet-}$ radical anion part. On longer time scales we observe intramolecular recombination. For E6 in methyl acetate (blue), the decay reflects the lifetime of the initially populated S_1/ICT state (140 ps).

At 760 nm (B), the rise of the transient signal for E6/TiO_2 (black) is due to formation of the long-lived $pTAA^{\bullet+}$–D49–pTAA species. We note that this is the wavelength for the band peak of this species in a nitrogen atmosphere (PSCP experiments), whereas for contact with acetonitrile a blue-shift of 40 nm is observed in the spectroelectrochemistry experiments (Fig. S7). For E6 on Al_2O_3 (red), the slow decay again reflects intramolecular recombination of the $pTAA^{\bullet+}$–$D49^{\bullet-}$–pTAA species. The transient for E6 in methyl acetate (blue) exhibits a fast initial change from absorption to stimulated emission, indicative of a transient Stokes shift (solvation). The signal then decays with the S_1/ICT lifetime of 140 ps.

The kinetics in the NIR at 1400 nm (C) for E6/TiO_2 (black) shows a fast decay due to the conversion of the initially prepared pTAA–$D49^{\bullet+}$–pTAA...e^- complex to $pTAA^{\bullet+}$–D49–pTAA *via* the parallel channels shown in Fig. 4(A) of the main manuscript. The weak residual absorption is due to conduction band electrons in TiO_2. They recombine with $pTAA^{\bullet+}$–D49–pTAA on a much longer time scale, so the signal stays constant in the 1 ns time window shown here. On Al_2O_3 (red), the very fast decay arises from conversion of the S_1/ICT state into the radical cation – radical anion species $pTAA^{\bullet+}$–$D49^{\bullet-}$–pTAA. The latter has no spectral band in the NIR. In methyl acetate (blue), the fast early loss in amplitude is due to solvation dynamics (blue-shift of the ESA band, see Fig. S11, second panel) and the slower subsequent decay with 140 ps is due to IC from the S_1/ICT state to S_0.

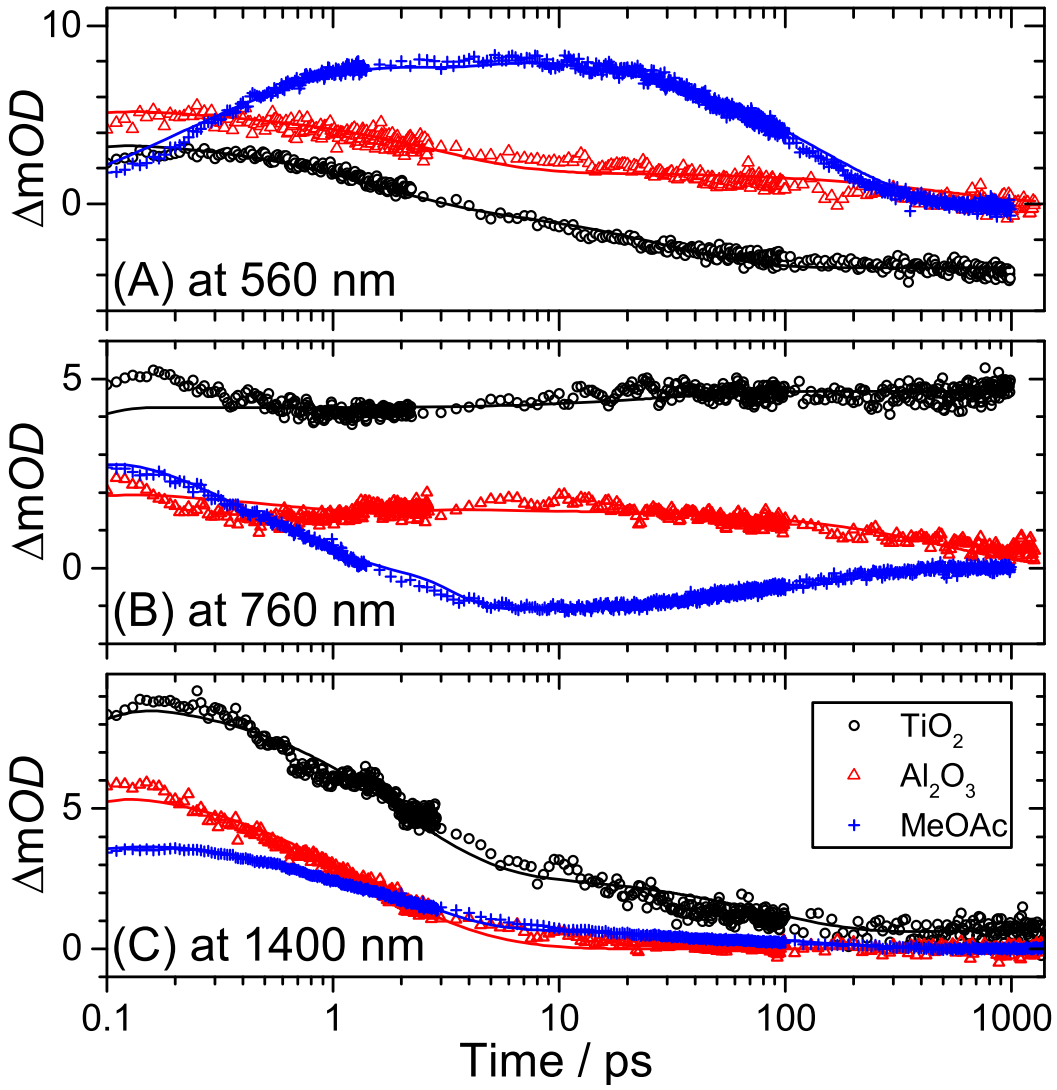

Fig. S12 Kinetic traces for E6 on TiO_2 (black), Al_2O_3 (red) and in methyl acetate (blue) including fit lines. (A) at 560 nm, (B) at 760 nm and (C) at 1400 nm. Note the logarithmic time scale.

Global kinetic analysis

Figure S13 shows results of the global kinetic analysis for E6 on TiO_2 in contact with N_2. Photoexcitation prepares the pTAA–D49$^{\bullet+}$–pTAA...e^-...TiO_2 complex at very early times (0.1 ps, magenta line). This complex decays *via* two parallel pathways: Synchronous electron transfer (τ_{1a} = 2.4 ps) involves electron injection into the TiO_2 conduction band, and fast hole transfer to the pTAA unit results in formation of the pTAA$^{\bullet+}$–D49–pTAA species (1.7 ps, green line) already at early times (note the "sharpening" of the pTAA$^{\bullet+}$ fingerprint band at 760 nm). In the "sequential" pathway, electron injection into the conduction band of TiO_2 occurs first (τ_{1b} = 3.9 ps), forming the core-oxidised species pTAA–D49$^{\bullet+}$–pTAA (1.7 ps, blue line). At 5 ps (3rd panel), the complex has almost completely decayed, and the dynamics is dominated by slower further build-up of pTAA$^{\bullet+}$–D49–pTAA by hole transfer at the expense of pTAA–D49$^{\bullet+}$–pTAA (τ_2 = 30 ps). At long times (4th panel) the only remaining radical cation species is pTAA$^{\bullet+}$–D49–pTAA, with a very sharp pTAA$^{\bullet+}$ feature at 760 nm. The weak absorption in the NIR is due to electrons in the TiO_2 conduction band.

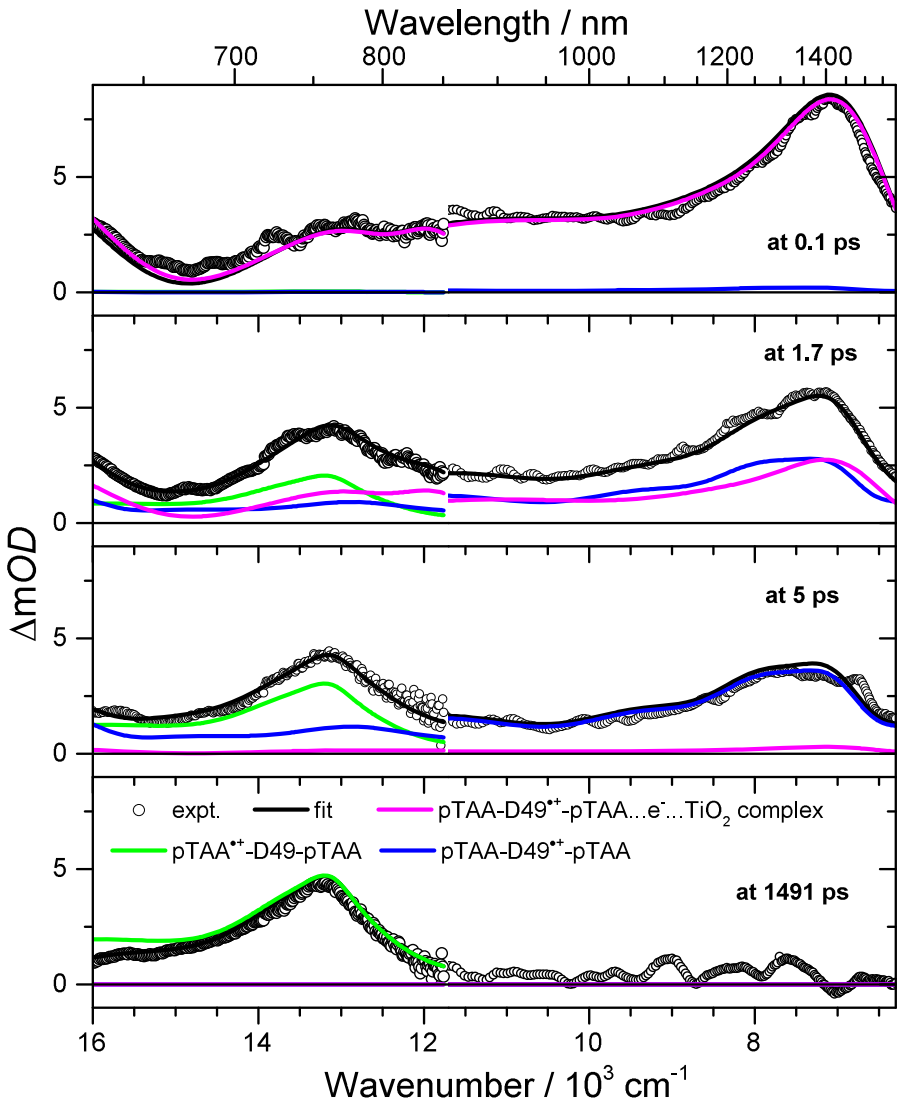

Fig. S13 Global analysis of PSCP transient absorption spectra of E6/TiO_2 in contact with N_2 showing representative fits at 0.1, 1.7, 5 and 1491 ps (from top to bottom).

Transition densities for the excited singlet states of E6

Figure S14 shows a plot of the transition densities of the fifteen lowest excited electronic states of E6 (S_1-S_{15}) for the MPW1K functional. S_1 is the bright state in the steady-state absorption experiments (pure D49 excitation), whereas S_2 and S_3 are optically dark transitions (zero orbital overlap) describing the transfer of an electron from one of the pTAA units to the D49 unit. Note that the particle densities (red) for S_1, S_2 and S_3 are identical, indicating that these three transitions share the same upper state.

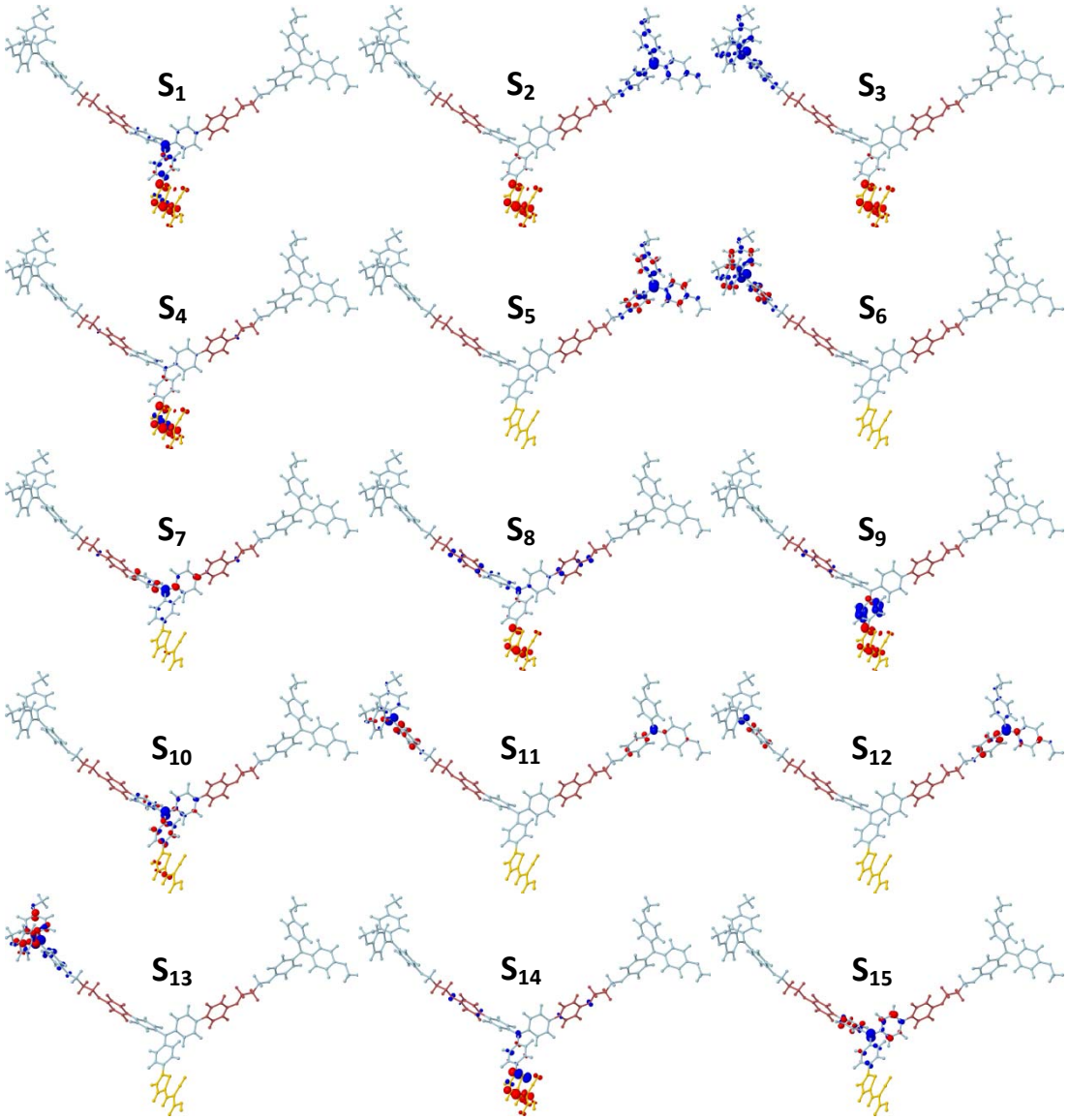

Fig. S14 Transition densities for the fifteen lowest electronically excited singlet states of E6 in vacuum from TDDFT calculations employing the MPW1K functional. Hole densities are drawn in blue, whereas particle densities are drawn in red.

Results of DFT/TDDFT calculations for different functionals

Table S1 contains electronic transition energies (divided by *hc*) and oscillator strengths *f* of the three energetically lowest electronic transitions of E6 for a wide range of functionals. A plot of the corresponding energy levels was shown in Fig. 5(A) (main manuscript). The transitions with zero oscillator strength originating from the pTAA units become the lowest energy transitions starting from the B97-3 functional onwards. The oscillator strength of the bright state systematically decreases with decreasing transition energy.

Table S1 Wavenumber $\tilde{\nu}$ and oscillator strength f from DFT/TDDFT calculations with TDA for the three energetically lowest excited singlet state transitions of E6 ($S_0 \rightarrow S_n$, n = 1-3) in vacuum using different functionals. In the case of the MPW1K, B97-3 and MPW1PW91 functionals, results are also provided for methyl acetate (C-PCM solvent model). DFT calculations of the S_0 structure employed B3LYP and a 6-31G(d) basis set. A 6-31+G(d) basis set was used in the TDDFT-TDA calculations, except for the MPW1K (6-31+G(d,p)) and B3LYP (6-31G(d)) functionals.

	$S_0 \rightarrow S_1$		$S_0 \rightarrow S_2$		$S_0 \rightarrow S_3$	
Functional	$\tilde{\nu}$ / cm^{-1}	f	$\tilde{\nu}$ / cm^{-1}	f	$\tilde{\nu}$ / cm^{-1}	f
wB97x	26651	1.6	34070	0.0	34095	0.1
LRC-wPBEh	25215	1.6	32157	0.0	32177	0.0
CAM-B3LYP	24205	1.4	30485	0.0	30753	0.0
BHHLYP	24112	1.4	28003	0.0	28258	0.0
MPW1K (vacuum)	22947	1.3	24517	0.0	24760	0.0
MPW1K (MeOAc)	21520	1.3	24865	0.0	24984	0.0
B97-K	22700	1.2	24166	0.0	24409	0.0
SOGGA11-X	22419	1.2	23242	0.0	23482	0.0
B97-3 (vacuum)	17423	0.0	17639	0.0	19695	0.9
B97-3 (MeOAc)	17589	0.0	17682	0.0	18219	1.0
MPW1PW91 (vacuum)	16558	0.0	16775	0.0	19283	0.9
MPW1PW91 (MeOAc)	16724	0.0	16818	0.0	17822	1.0
B97-2	15004	0.0	15216	0.0	18498	0.8
B3LYP	14858	0.0	15060	0.0	18550	0.8
LB94	5848	0.0	6027	0.0	12923	0.5

Influence of S_0 structure and Tamm-Dancoff approximation (TDA)

In Fig. 5 (B) of the main manuscript we showed that a systematic variation of the amount of HF exchange in the functional leads to a systematic change in the relative positions of the D49 and pTAA levels. In Fig. S15 (A) we used the TDA as in Fig. 5(B), but the fixed S_0 structure from B3LYP calculations was employed instead of optimising the S_0 structure for each respective functional. Except for a weak decrease of all transition energies (Table S2), the observed trends and the position of the "cross-over point" at *ca.* 37% HF exchange stay the same. In panel (B), the same calculations as in (A) were performed, but dropping the TDA. One observes a decrease in the transition energies of the D49-centred transitions by a slightly larger amount, but the observed trends still persist, with the cross-over point slightly shifted to *ca.* 34%. We conclude that the energetic changes in the D49 and pTAA transitions are largely controlled by the amount of HF exchange in the functional.

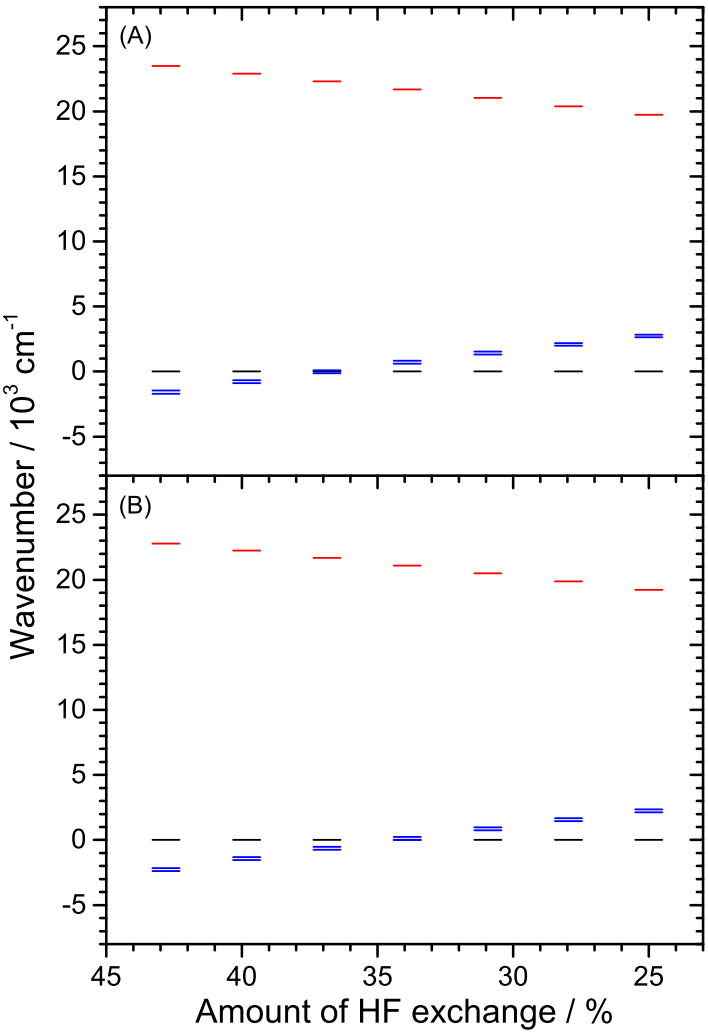

Fig. S15 TDDFT results for the dye E6 employing a systematic variation of the amount of HF exchange from 42.8% (MPW1K) to 25.0% (MPW1PW91). The other contributions in each of the functionals are mPW91 GGA exchange and PW91 GGA correlation. (A) With TDA. (B) Without TDA. In all cases, a fixed S_0 structure was used (B3LYP, 6-31G(d) basis set). The 6-31G(d) basis set was also used for the TDDFT-TDA calculations. The energy of the lower level (black) of the optically bright "D49 transition" is set to zero for an easier comparison.

Table S2 Wavenumber $\tilde{\nu}$ and oscillator strength f from DFT/TDDFT calculations for the three energetically lowest excited singlet state transitions of E6 ($S_0 \rightarrow S_n$, n = 1-3) in vacuum using different functionals. DFT calculations of the S_0 structure employed a 6-31G(d) basis set and either B3LYP for "TDA(B)" and "NoTDA(B)" or the respective functional given in the first column of the table for "TDA(R)". A 6-31G(d) basis set was used in all excited-state calculations. In the case of "NoTDA(B)" the Tamm-Dancoff approximation was dropped.

Amount of HF exchange / %	$\tilde{\nu}$ **($S_0 \rightarrow S_1$)/ cm^{-1}**			$\tilde{\nu}$ **($S_0 \rightarrow S_2$)/ cm^{-1}**			$\tilde{\nu}$ **($S_0 \rightarrow S_3$)/ cm^{-1}**		
	TDA(R)	**TDA(B)**	**NoTDA(B)**	**TDA(R)**	**TDA(B)**	**NoTDA(B)**	**TDA(R)**	**TDA(B)**	**NoTDA(B)**
25.00 (MPW1PW91)	19917	19722	19222	17036	16880	16880	17188	17092	17092
27.96	20656	20386	19864	18430	18406	18406	18581	18189	18189
30.93	21398	21041	20491	19845	19515	19515	19995	19737	19737
33.90 ("MPW1$^{33.9}$PW91")	22135	21681	21101	21277	20853	20853	21426	21080	21078
36.86	22859	22230	21683	22719	22197	22198	22719	22429	22429
39.83	23585	22899	22243	24180	23557	23557	24328	23794	23794
42.80 (MPW1K)	24292	23473	22775	25656	24927	24927	25802	25169	25169

Comparison of structures for the ground electronic state S_0

Figure S16 compares the optimised geometries of the ground electronic state S_0 of E6 from DFT calculations. The blue, red and green structures are obtained using the B3LYP, MPW1K and "MPW1$^{33.9}$PW91" (33.9% HF exchange) functionals. The molecular geometries in XYZ format can be found in the second ESI file. The structures largely agree and therefore support the result found in Fig. S15 that functional-induced structural differences of the S_0 state have only a weak influence on the transition energies. Minor variations in the S_0 structure are only found in the region of the pTAA substituents which are attached *via* flexible diether chains, resulting in a relatively flat potential for torsional motion.

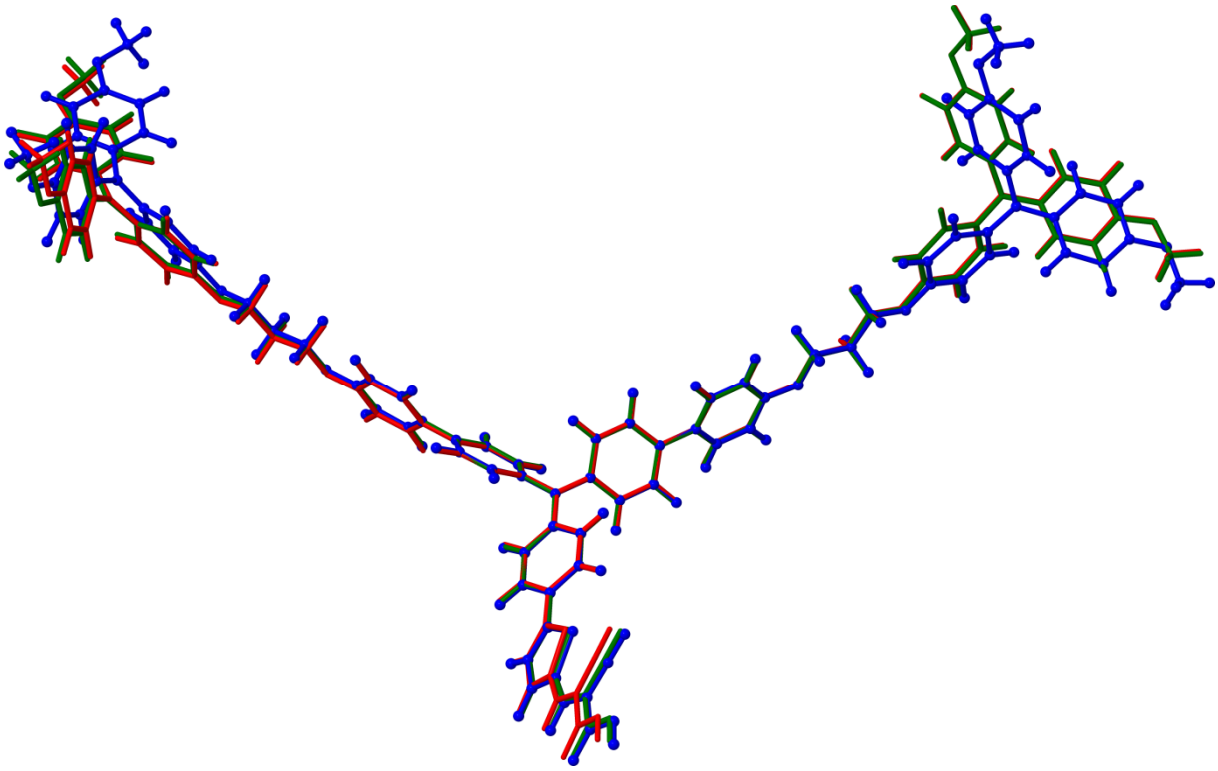

Fig. S16 Overlay of geometries for the ground electronic state S_0 of E6 from DFT calculations using the functionals B3LYP (blue), MPW1K (red) and "MPW1$^{33.9}$PW91" (green).

Singlet transitions of E6 in vacuum and methyl acetate

Table S3 contains electronic transition energies (divided by *hc*) and oscillator strengths *f* of E6 for the optimised "MPW1[33.9]PW91" functional in vacuum and methyl acetate. A comparison of these values with the steady-state absorption spectra of E6, D49 and pTAA is included in Fig. 6 (A)-(C) of the main manuscript.

Table S3 Wavenumber $\tilde{\nu}$ and oscillator strength *f* from DFT/TDDFT calculations with TDA for $S_0 \rightarrow S_n$ singlet transitions of E6 in vacuum and methyl acetate. Transitions involving only the pTAA substituents are highlighted as bold blue numbers.

n	Vacuum		Methyl acetate	
	$\tilde{\nu}$ / cm^{-1}	*f*	$\tilde{\nu}$ / cm^{-1}	*f*
1	20906	0.00	20236	1.07
2	21067	0.00	21099	0.00
3	21656	1.00	21156	0.00
4	29641	0.76	28512	0.65
5	**29955**	**0.03**	29431	0.04
6	**29972**	**0.03**	**29834**	**0.05**
7	30351	0.03	**29843**	**0.04**
8	31157	0.67	30931	0.87
9	31794	0.29	31786	0.13
10	32851	0.14	32286	0.22
11	33230	0.00	33641	0.11
12	33327	0.00	**34069**	**0.39**
13	33859	0.00	**34077**	**0.46**
14	33980	0.00	**34101**	**0.35**
15	**34400**	**0.31**	**34101**	**0.33**
16	**34408**	**0.33**	34400	0.00
17	34512	0.00	34448	0.00
18	34521	0.02	34577	0.00
19	**34545**	**0.26**	34633	0.00
20	**34553**	**0.26**	34722	0.00
21	34617	0.01	34779	0.00
22	34674	0.06	34980	0.00
23	34771	0.03	34988	0.00
24	35206	0.00	35513	0.02
25	35343	0.00	**35972**	**0.12**
26			**35972**	**0.15**
27			**35988**	**0.14**
28			**35988**	**0.11**
29			36351	0.04
30			36626	0.00

Comparison of S_0 and S_1 structures

Figures S17 and S18 contain overlays of the relaxed S_0 (red) and S_1 (green) structures for the optimised "MPW1$^{33.9}$PW91" functional. The molecular geometries in XYZ format can be found in the second ESI file. As the most prominent difference, relaxation in the S_1 state leads to planarisation of the thiophenyl unit and the adjacent aryl group of the triarylamine electron donor group of the D49 chromophore. The planarisation of both groups with respect to each other is most easily seen in Fig. S18. Here the view goes along the bond connecting both groups located in the center of the picture.

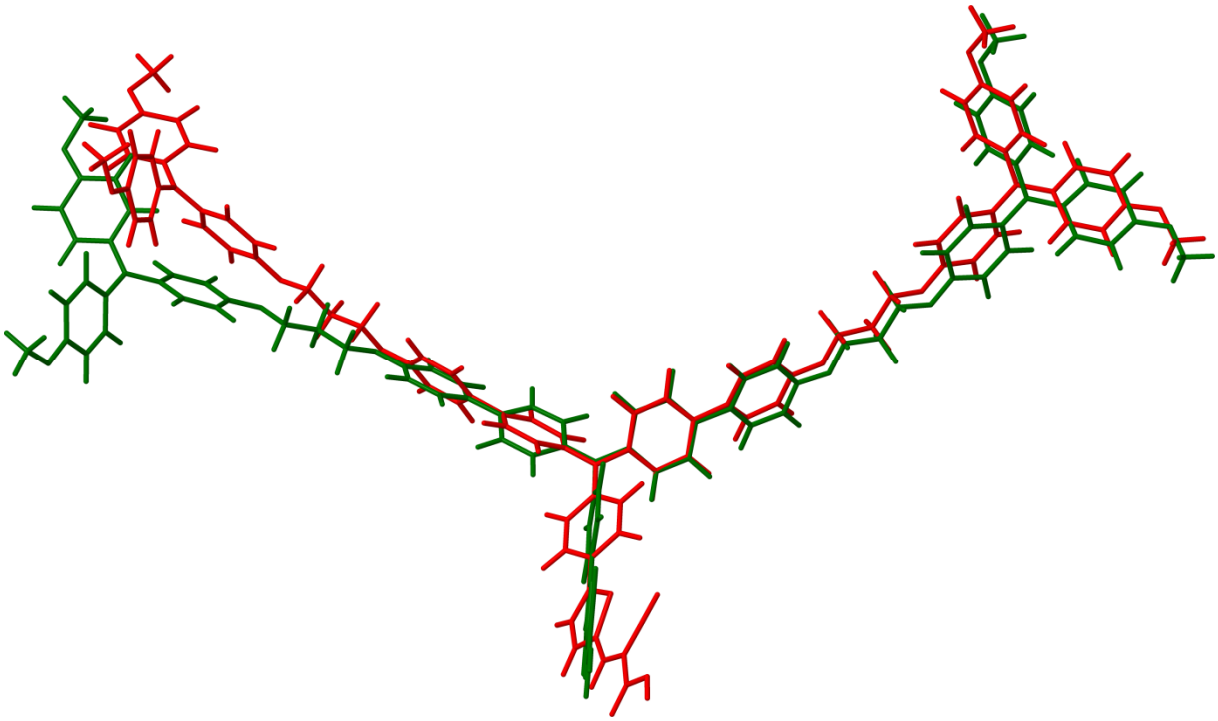

Fig. S17 Geometries of the S_0 (red) and S_1 (green) states from DFT/TDDFT calculations using the functional "MPW1$^{33.9}$PW91".

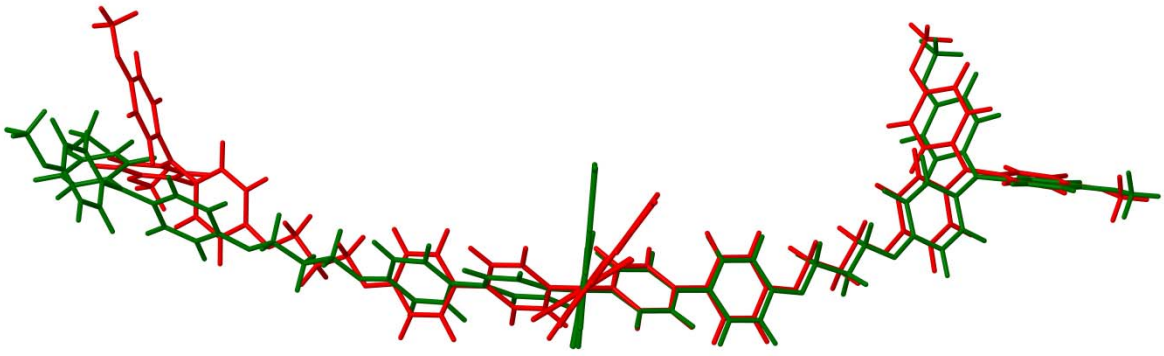

Fig. S18 Same as in Fig. S17, but viewing along the bond connecting the thiophenyl group and the adjacent triarylamine group of the D49 chromophore unit. The planarisation of the two groups in S_1 (green) is clearly seen in the centre of the picture.

Contour plots of PSCP spectra for E6 and D49 in methyl acetate

Figure S19 shows a comparison of contour plots for PSCP spectra of the E6 dye (top) and the D49 dye (bottom) in methyl acetate after excitation with a laser pulse centred at 505 nm. The spectra are virtually indistinguishable and prove that the dynamics in organic solvents reflects pure relaxation of the initially excited D49 core chromophore. Both pTAA units of E6 are not involved in the dynamics and therefore in this organic solvent the formation of the radical cation – radical anion species $pTAA^{\bullet+}$–$D49^{\bullet-}$–pTAA by intramolecular hole transfer does not occur.

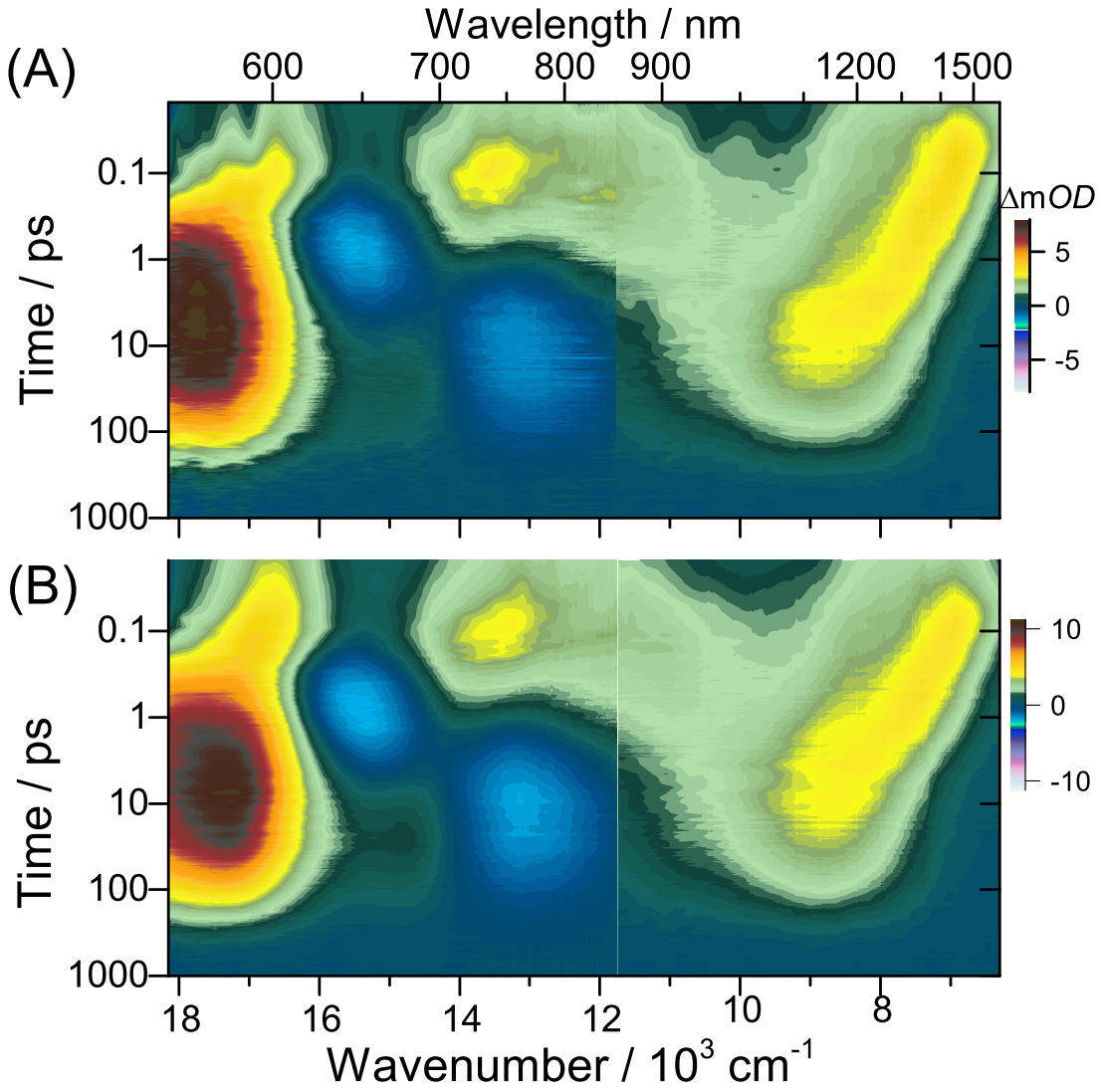

Fig. S19 Contour plots of transient broadband absorption spectra of E6 (A) and D49 (B) in methyl acetate. Note the logarithmic time scale.

References

1. K. Oum, O. Flender, P. W. Lohse, M. Scholz, A. Hagfeldt, G. Boschloo and T. Lenzer, *Phys. Chem. Chem. Phys.*, 2014, **16**, 8019.
2. O. Flender, M. Scholz, J. R. Klein, K. Oum and T. Lenzer, *Phys. Chem. Chem. Phys.*, 2016, **18**, 26010.
3. Y. Hao, E. Gabrielsson, P. W. Lohse, W. Yang, E. M. J. Johansson, A. Hagfeldt, L. Sun and G. Boschloo, *Adv. Sci.*, 2015, **2**, 1500174.
4. V. V. Pavlishchuk and A. W. Addison, *Inorg. Chim. Acta*, 2000, **298**, 97.
5. S. Amthor, B. Noller and C. Lambert, *Chem. Phys.*, 2005, **316**, 141.